QUANTITATIVE ANALYSIS OF MULTILAYER SAMPLES IN INTEGRAL CONVERSION ELECTRON MÖSSBAUER SPECTROSCOPY (ICEMS).*

Francesc SALVAT

Departament d'Estructura i Constituents de la Matèria.
Facultat de Física. Universitat de Barcelona.
Diagonal 645. 08028 Barcelona. Spain.

ABSTRACT.

A practical method for quantitative analysis of multilayer samples using integral conversion electron Mössbauer spectroscopy (ICEMS) is described. The method is based on a theoretical approach allowing the calculation of ICEMS area percentages in terms of a small number of physical parameters characterizing each phase in the sample. The model equations can be easily incorporated in a computer program to give estimates of the mass-thickness of the sample layers through numerical fitting of the computed area percentages to the measured ones.

RESUM.

Es descriu un procediment per a l'anàlisi quantitativa de mostres estratificades a partir de l'espectre Mössbauer amb electrons de conversió (ICEMS). El mètode es basa en un model teòric que permet calcular els percentatges d'àrea en termes d'un petit nombre de paràmetres que caracteritzen les diferents fases de la mostra. Les equacions del model es poden incorporar en un programa d'ordinador que proporcioni estimacions dels gruixos de les làmines de la mostra per ajust numèric dels percentatges d'àrea.

* Supported in part by the Comisión Asesora de Investigación Científica y Técnica (Spain), contract n. 2157/83.

1. INTRODUCTION.

In recent years, Integral Conversion Electron Mössbauer Spectroscopy (ICEMS) has been efficiently used for studying the chemical and physical structure of the surface region of samples containing ^{57}Fe and ^{119}Sn. In an ICEMS measurement, a collimated beam of resonant gamma radiation coming from the Mössbauer source impinges on the surface of the absorber. The spectrum is obtained by collecting essentially all the electrons leaving the surface of the absorber by using a proportional detector (usually a flow proportional counter similar to that described by Swanson and Spijkerman [1]). The detected electrons are due to photoelectric effect of all the radiations coming from the source and to resonant absorption of the incoming recoilless gamma radiation. The photoelectrons are mainly responsible for the observed background, whereas the "resonant" electrons give rise to the Mössbauer signal. In fact, only those electrons emitted at depths lower than the corresponding Bethe range can reach the detector and the recorded spectrum is strongly weighted in favour of the surface region. Extensive reviews on the fundamentals and applications of CEMS have been published by Tricker [2] and Liljequist [3].

In the cases where quantitative analysis makes sense, the surface region of the absorber contains a number of different phases, each of which gives rise to a distinguishable partial spectrum. The composition of each one of the present phases can usually be obtained from the structure of the measured spectrum and from available information about the chemical processes undergone by the sample. The aim of the theory is to determine the distribution and thicknesses of the present phases from the measured spectrum on the assumption that the surface region has a multilayer structure. Although only a small number of quantitative studies have been done to date owing to the lack of a general method of analysis, the ICEMS spectra contains valuable information on the quantitative composition of the sample which can be obtained by using relatively simple procedures.

The basic quantities in the analysis are the percentage

signals, i.e. the area percentage under each partial spectrum, which can be computed by using theoretical methods if the composition and ordering in depth of the different phases in the sample are known. The possibility of quantitative analysis through numerical fitting of the theoretical area percentages to the measured ones was opened up ten years ago with several theoretical works aimed at describing the generation and transport of electrons inside the sample. The first attempts in quantitative analysis were done by Simmons et al. [4] and by Huffman and Podgurski [5], who applied simple theoretical approaches to study the oxidation rate of metallic iron targets. However, their quantitative results are questionable due to inaccuracies of the theory. Since then, the relevant mechanisms involved in the electron generation, transport and detection have been better understood and included in the theoretical work of Salvat and Parellada [6] which provides a suitable basis for quantitative use of ICEMS.

The de-excitation of the Mössbauer nuclei after resonant absorption of a gamma ray in the primary beam (coming from the source) takes place by emission of either a gamma ray (secondary gamma radiation) or a conversion electron (primary conversion electron or PCE). Table I shows the kind of the main radiations emitted in the nuclear de-excitation of $^{57}Fe^{*}$ and $^{119}Sn^{*}$, as well as their energies and emission probabilities (see appendix A). After the internal conversion process, the energy excess of the atom is given off with emission of Auger electrons (primary Auger electrons or PAE) and/or X-rays (secondary X radiation). Usually the major part of the ICEMS signal is due to primary electrons (PCE and PAE) and the rest of the signal is due to secondary electrons emitted by photoelectric effect, or after resonant absorption, of secondary X or gamma radiation. Thus, the secondary electrons are: gamma photoelectrons (GPE), X photoelectrons (XPE), secondary conversion electrons (SCE) and secondary Auger electrons (SAE). From the data in table I, it can be shown that the contribution to the ICEM signal of processes involving three consecutive resonant absorptions inside the absorber is negligible (see also appendix A).

Kind of radiation	Energy (keV)	Emission probability	Bethe range (mg/cm_2)
^{57}Fe			
Resonant gamma ray	E_0=14.4	w_0=0.104	0.799
K shell IC electron	e_1=7.3	u_1=0.802	0.260
KL-L Auger electron	e_1'=5.4	u_1'=0.529	0.160
K X ray	E_1=6.3	w_1=0.273	0.205
L shell IC electron	e_2=13.6	u_2=0.082	0.726
M shell IC electron	e_3=14.3	u_3=0.012	0.790
Other electrons and X rays	<0.8	≈0.896	
^{119}Sn			
Resonant gamma ray	E_0=23.8	w_0=0.164	1.871
L shell IC electron	e_1=19.6	u_1=0.836	1.345
LM-M Auger electron	e_1'=2.8	u_1'=0.736	0.058
X ray	E_1=3.6	w_1=0.100	0.085
Other electrons and X rays	<1.0	≈ 0.836	

Other data	^{57}Fe	^{119}Sn
Resonant cross section σ_0 (cm^2)	$2.56\ 10^{-18}$	$1.42\ 10^{-18}$
Natural level width Γ_0 (mm/s)	$9.7\ 10^{-2}$	$3.1\ 10^{-1}$
K shell partial ICC	7.675	-------
L shell partial ICC	0.784	5.08
M shell partial ICC	0.115	-------
Total IC coefficient	8.574	5.08
Fluorescence yields	$(FY)_K$=0.34	$(FY)_L$=0.12

TABLE I. Characteristics of the main radiations emitted in the deexcitation of $^{57}Fe^*$ and $^{119}Sn^*$. Resonant total cross sections and natural level widths are also included.

In practice not all the electrons leaving the surface of the absorber can be effectively detected because of the coincidence effect [7]: when several electrons enter the detector in a time interval that is smaller than the detector dead time, only a single pulse is obtained. In an actual experiment, all the radiations emitted in a single nuclear de-excitation are expelled from the Mössbauer atom in a time interval that is much shorter than the detector dead time, and this coincidence effect reduces the magnitude of the ICEMS signal. The largest number of coinciding events occur when a conversion electron enters into the detector followed by its subsidiary Auger electron (see table I). As the existing theories take into account only the coincidences between these correlated pairs of electrons, the coincidence effect is also referred to as pairing effect. There are also coincidences between correlated PCE and XPE. However, as the photoelectric absorption coefficient of the secondary X rays is very small as compared with the inverse Bethe range of the PCE, the effect of the PCE and XPE coincidences is negligible.

As pointed out by Liljequist [8], the coincidence effect reduces the error introduced by ignoring the contributions to the ICEMS signal of the low energy electrons and X rays resulting from the final states of the Auger cascade. These Auger electrons and the corresponding XPE can reach the detector only if they start from very near the surface and are always correlated with some higher energy electron. Thus they are to some extent shadowed by the coincidences.

The magnitudes of the effect and the background are not independent. Because of the resonant absorption of the recoilless gamma radiation coming from the source, the background usually shows a small decrease under the scattering peaks, and the effective intensity of the peaks in the spectrum is reduced. As a consequence, the background is independent of the source velocity only far from the resonance peaks. For samples with natural abundance of the Mössbauer isotope, the attenuation of the incident beam due to resonant absorption at a depth of the order of the Bethe ranges is small and the relative reduction of the ICEMS signal due to this

effect is practically negligible. However, this background reduction becomes noticeable for enriched samples and must be introduced into the theory if quantitative analysis is attempted.

The first theories for the quantitative interpretation of ICEMS measurements were developed by Krakowski and Miller [9], Bainbridge [10] and Huffman [11]. In all these theories, only the part of the signal due to primary electrons is taken into account and the weight function, which describes the attenuation of the emerging electron flux, is derived from the empirical formula of Cosslett and Thomas [12]. The effect of the secondary electrons was experimentally demonstrated by Tricker et al. [13] and incorporated in the theory by Liljequist et al. [14] who used a more realistic weight function derived from Monte Carlo calculations. More recently, Deeney and McCarthy [7] have taken into account the coincidence effect and have removed some simplifications made by Liljequist et al. [14]. A similar approach has been used by Liljequist [8,15] to simulate partial signals of duplex non-enriched absorbers. Salvat and Parellada [6] have reformulated the general theory for multilayer samples including a realistic description of: i) the attenuation of the primary beam, ii) the generation of secondary electrons, iii) the coincidence effect and iv) the background correction. This last version of the theory gives rise to rather complicated expressions for the so called "spectral functions", which play the central role in the quantitative analysis of the sample from the measured spectrum. It uses the weight function derived by Liljequist [8]. More realistic weight functions have been computed recently by Salvat et al. [16] from a more accurate Monte Carlo method.

In this work, the general theory [6] is improved, by using these last weight functions, and largely simplified, by introducing a suitable analytical approximation to describe the flux attenuation of secondary radiations. In this way, analytical expressions of the spectral functions for multilayer samples are derived. The ICEMS signal of each layer in the absorber is given as the integral of the corresponding spectral function. Although the computation of this integral may require a large amount of numerical work, the use of suitable numerical methods reduces this work to reasonable

limits. The ability of the theory for quantitative study of multilayer samples is evidenced here by comparing theoretical and experimental results for absorbers of known composition [1,17,18].

2. OVERVIEW.

The problem we deal with is shown schematically in fig. 1. A collimated beam of resonant gamma radiation coming from a Mössbauer source impinges on the surface of an ideal multilayer absorber with NL different layers of mass thicknesses $X^{(1)}$, $X^{(2)}$, ..., $X^{(NL)}$ (g/cm^2). The materials and/or the concentrations of resonant nuclei can be different for each layer. In the following we shall use upper indices between brackets to distinguish among the different layers in the sample.

We wish to calculate the total number of electrons leaving the surface of the absorber per unit time as a function of the source velocity v. Except from a multiplicative constant, this number coincides with the number of counts in the corresponding channel of the measured spectrum.

Let I_0 be the number of resonant gamma rays which, coming from the Mössbauer source, cross the surface of the sample per unit time. The energy distribution of the recoilless gamma radiation is given by

$$RI^{(0)}(E,v)\, dE = I_0\, f_s\, L(E,v)\, dE \ . \qquad (1)$$

f_s being the source recoilless fraction and

$$L(E,v) = \frac{2}{\pi\, \Gamma_s} \frac{(\Gamma_s/2)^2}{(\Gamma_s/2)^2 + [E-E_0(1+v/c)]^2} \qquad (2)$$

a lorentzian distribution. E_0 is the excitation energy of the source nuclei, Γ_s is the width (FWHM) of the source emission line and c is the speed of light. It is convenient to introduce the reduced energy $y \equiv 2(E-E_0)/\Gamma$ and the reduced velocity $s \equiv 2v/\Gamma_0$, where Γ is the natural level width and $\Gamma_0 \equiv c\Gamma/E_0$. Eq. (1) can be written in terms of these dimensionless variables as

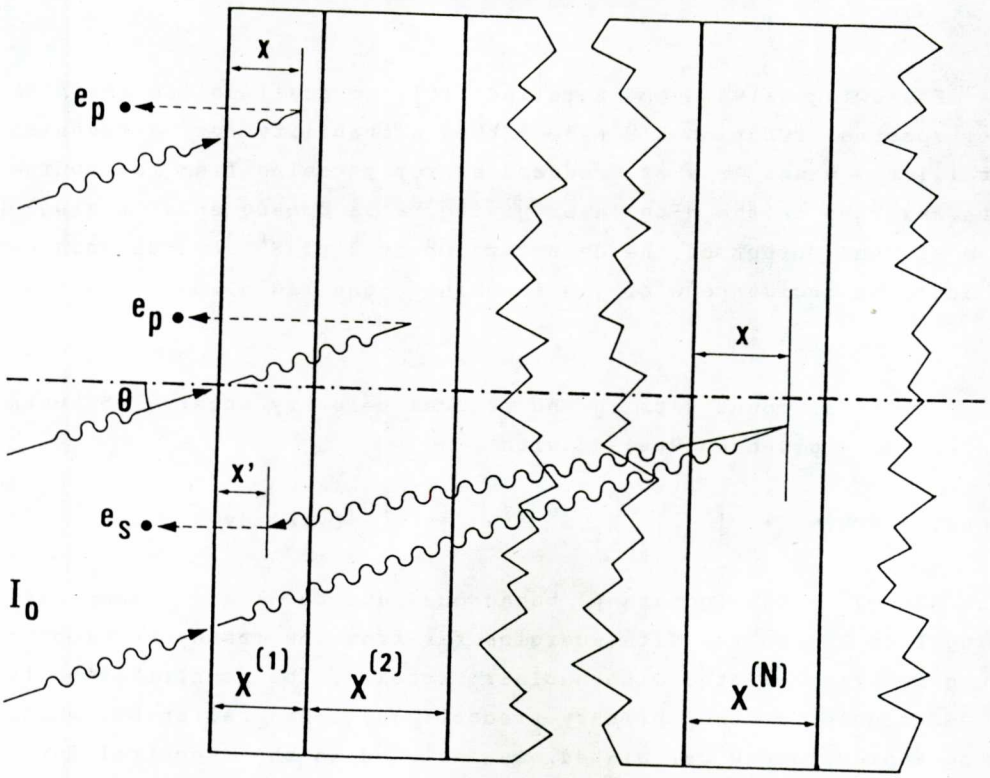

FIGURE 1. Schematic representation of the geometry in an ICEMS measurement. The generation mechanisms of primary (e_p) and secondary (e_s) electrons are indicated. Notice that the generation depth of secondary electrons is denoted x'.

$$RI^{(0)}(y,s)\,dy = I_0\, f_s\, L(y,s)\,dy \tag{3}$$

with

$$L(y,s) = \frac{\gamma_s}{\pi}\,\frac{1}{1+\gamma_s^2\,(y-s)^2} \tag{4}$$

and $\gamma_s \equiv \Gamma/\Gamma_s$.

Following Salvat and Parellada [6], we shall define the N-th layer spectral function $S^{(N)}(y)$ as the probability for a resonant (recoilless) gamma ray of reduced energy y coming from the source to be absorbed in the N-th layer giving, as a consequence, a single pulse at the output of the detector. Obviously, $S^{(N)}(y)$ depends on the angle of incidence θ of the incoming gamma radiation (see fig. 1).

The total count rate in the reduced velocity interval between s and s+ds is given by N(s)·ds with

$$N(s) = NRB(\infty) + \int_{-\infty}^{\infty} \left[\sum_{N=1}^{NL} S^{(N)}(y) \right] RI^{(0)}(y,s)\,dy \tag{5}$$

where NRB(∞) is the (constant) background due to X and gamma rays coming from the source with energies far from the resonance (including gamma rays emitted with nuclear recoil). The contribution to the background of the primary (recoilless) gamma radiation, which can be approximately calculated, is included in the spectral functions. For photon energies far from the resonance energies, the spectral functions become independent of the reduced energy. Thus it is useful to introduce a new set of spectral functions $SPC^{(N)}(y)$ by subtracting the asymptotic value:

$$SPC^{(N)}(y) \equiv S^{(N)}(y) - S^{(N)}(\infty). \tag{6}$$

Clearly, these functions coincide with those defined in ref. [6]. In terms of these functions, the total count rate can be written as

$$N(s) = \left[\sum_{N=1}^{NL} NE^{(N)}(s) \right] + TB(\infty) \tag{7}$$

where

$$NE^{(N)}(s) = \int_{-\infty}^{\infty} SPC^{(N)}(y)\, RI^{(0)}(s,y)\, dy \qquad (8)$$

is the contribution to the effect due to gamma rays absorbed in the N-th layer, i.e. the partial spectrum, and

$$TB(\infty) = NRB(\infty) + I_0\, f_s \sum_{N=1}^{NL} S^{(N)}(\infty) \qquad (9)$$

is the total background (which can only be experimentally determined).

Actually, the energy spectrum of the primary radiation (3) depends only on the dimensionless variable s-y. Thus, if $\Omega(s-y) \equiv L(s,y)$, eq. (8) reduces to

$$NE^{(N)}(s) = I_0\, f_s\, SPC^{(N)}(s) \text{ xo } \Omega(s), \qquad (10)$$

i.e. the partial spectra $NE^{(N)}$ can be written as the convolution product of the source emission spectrum and the spectral function $SPC^{(N)}$. Evidently, the same result holds for multiline sources.

The spectral area, given by

$$A_{tot} = \frac{1}{TB(\infty)} \int_{-\infty}^{\infty} [NE(s)-TB(\infty)]\, ds, \qquad (11)$$

can be written as the sum of the areas contributed by each layer in the sample, i.e.

$$A_{tot} = \sum_{N=1}^{NL} A^{(N)} \qquad (12)$$

with

$$A^{(N)} = \frac{I_0\, f_s}{TB(\infty)} \int_{-\infty}^{\infty} SPC^{(N)}(y)\, dy. \qquad (13)$$

The most basic quantities experimentally determined are the area percentages (or percentage signals)

$$AP^{(N)} = 100\, A^{(N)} / A_{tot} \qquad (14)$$

and relative signals

$$RS^{(N,L)} \equiv A^{(N)} / A^{(L)}. \qquad (15)$$

These quantities, being independent of the spectral background TB(∞), can be easily computed from the spectral functions.

3. SPECTRAL FUNCTIONS.

In order to compute the spectral functions $S^{(N)}(y)$, we shall consider a primary beam in which only a gamma ray of reduced energy y enters into the absorber per unit time. In this case, $S^{(N)}(y)$ coincides with the detector counting rate due to those primary gamma rays which have been absorbed in the N-th layer.

3.1. PHOTON TRANSPORT.

Gamma radiations in the energy range involved in Mössbauer spectroscopy can interact with the absorber through two kinds of processes: a) non-resonant or conventional interactions (photoelectric and Compton effects), and b) nuclear resonant absorption (Mössbauer effect).

The gamma ray absorption at the N-th layer due to nonresonant processes can be described by a mass absorption coefficient $\mu_0^{(N)}$ which, in the energy range swept by Doppler effect, is independent of the energy and practically coincides with the photoelectric mass absorption coefficient. Accurate values of the mass absorption coefficient for photons of energy E in single element materials can be found from theoretical calculations [19], or easily evaluated using semiempirical formulae [20] or interpolated from experimental results. For compound materials or alloys $\mu(E)$ is, to a good approximation, additive:

$$\mu(E) = \Sigma\, g_i\, \mu_i(E) \qquad (16)$$

where g_i is the mass fraction contributed by the element i with mass absorption coefficient $\mu_i(E)$ and the summation covers all constituent elements [20].

The nuclear resonant absorption cross-section at the N-th layer is given by the Breit-Wigner formula. In the most general case, the absorber nuclei can show hiperfine splittings. Thus, if $E_j^{(N)}$ and $\Gamma_j^{(N)}$ are the position and width of the j-th resonance, the resonant absorption can be characterized by a mass absorption coefficient [6]

$$\mu_R^{(N)}(y) = \frac{n^{(N)}}{\rho^{(N)}} f^{(N)} \sigma_0 \sum_j \frac{\beta_j^{(N)}}{1 + [2(E-E_j^{(N)})/\Gamma_j^{(N)}]^2} . \qquad (17)$$

$\rho^{(N)}$, $n^{(N)}$, and $f^{(N)}$ are the mass density, the resonant nuclei concentration and the recoil-free fraction (or Debye-Waller factor) of the N-th layer material. σ_0 is the total resonant cross-section and $\beta_j^{(N)}$ is the statistical weight of the j-th resonance. The mass absorption coefficient (17) can be written in terms of the reduced energy y as

$$\mu_R^{(N)}(y) = t_0^{(N)} \sum_j \frac{\beta_j^{(N)}}{1 + [\gamma_j^{(N)}(y-s_j^{(N)})]^2} \qquad (18)$$

where

$$t_0^{(N)} = n^{(N)} f^{(N)} \sigma_0 / \rho^{(N)} \qquad (19)$$

is the effective thickness per unit length,

$$\gamma_j^{(N)} \equiv \Gamma / \Gamma_j^{(N)} \qquad (20)$$

and

$$s_j^{(N)} \equiv 2 v_j^{(N)} / \Gamma_0 , \qquad (21)$$

$v_j^{(N)}$ being the source velocity corresponding to the j-th resonance peak:

$$v_j^{(N)} = c [E_j^{(N)}/E_0 - 1] . \qquad (22)$$

The values of the parameters $\beta_j^{(N)}$, $\gamma_j^{(N)}$ and $s_j^{(N)}$ can be derived from the height, width and positions of the corresponding peaks in the measured spectrum after deconvolution with the source emission spectrum.

The number of gamma rays in the primary beam crossing a plane parallel to the surface at a depth x inside the N-th layer per unit time is given by

$$RI^{(N)}(y,x) = Q^{(N)}(x)\, R^{(N)}(y,x) \tag{23}$$

where the factors

$$Q^{(N)}(x) = \exp\{-\sec\theta \left[\sum_{L=1}^{N-1} \mu_0^{(L)} X^{(L)} + \mu_0^{(N)} x \right]\} \tag{24}$$

and

$$R^{(N)}(y,x) = \exp\{-\sec\theta \left[\sum_{L=1}^{N-1} \mu_R^{(L)}(y) X^{(L)} + \mu_R^{(N)}(y) x \right]\} \tag{25}$$

account for the attenuation of the primary beam due to conventional interactions and resonant absorption respectively. The rates of primary gamma rays absorbed at depths between x and x+dx in the N-th layer as a consequence of conventional interactions and resonant absorption are

$$\sec\theta\, \mu_0^{(N)}\, RI^{(N)}(y,x)\, dx \tag{26}$$

and

$$\sec\theta\, \mu_R^{(N)}(y)\, RI^{(N)}(y,x)\, dx \tag{27}$$

respectively. From now on, we shall drop the argument in the attenuation functions (24) and (25) when it takes its maximum value, i.e.

$$Q^{(N)} \equiv Q^{(N)}(X^{(N)}),\ R^{(N)}(y) \equiv R^{(N)}(y, X^{(N)}) \tag{28}$$

In each nuclear de-excitation, a gamma ray of energy near E_0 or X rays with characteristic energies E_1, E_2, ... can be emitted. Let w_0, w_1, ... be the corresponding emission probabilities (see table I and appendix A). The mass absorption coefficients for conventional interactions of these radiations with the material in the N-th layer will be represented by $\mu_0^{(N)}$, $\mu_1^{(N)}$, ...

Secondary gamma rays can also suffer nuclear resonant absorption in the sample. The L-th layer mass absorption

coefficient for secondary gamma radiation generated in the N-th layer is given by the conventional contribution, $\mu_0^{(N)}$, plus the resonant one. The latter is

$$\mu_{RS}^{(N,L)} = f^{(N)} \left[\pi \, t_0^{(N)} \sum_j \left(\beta_j^{(N)} / \tau_j^{(N)} \right) \right]^{-1} \int_{-\infty}^{\infty} \mu_R^{(N)}(y) \, \mu_R^{(N)}(y) \, dy \tag{29}$$

where the factor inside brackets normalizes the emission spectrum.

We shall assume that the emission of secondary radiation is isotropical. For a plane isotropical source of photons embedded in an infinite medium with mass absorption coefficient μ (cm^2/g) giving I(0) photons per unit time, the number of photons crossing a plane parallel to the source placed at a distance x (g/cm^2) per unit time is given by

$$I(\mu x) = \frac{I(0)}{2} e^{-\mu x} \left[1 - \mu x \, e^{\mu x} E_1(\mu x) \right] \tag{30}$$

where $E_1(\mu x)$ is the exponential integral function [21]. For multilayer samples, the argument μx in (30) has to be replaced by the effective thickness between the source and the plane. For each two layers, N and L, we define the functions

$$A_0^{(N.L)}(x,x') = \sum_J \left[\mu_0^{(J)} + \mu_{RS}^{(N,J)} \right] X^{(J)} + O(N,L) \left[\mu_0^{(N)} + \mu_{RS}^{(N,N)} \right] x - O(N,L) \left[\mu_0^{(L)} + \mu_{RS}^{(N,L)} \right] x' \tag{31a}$$

$$A_j^{(N,L)}(x,x') = \sum_J \mu_j^{(J)} X^{(J)} + O(N,L) \, \mu_j^{(N)} x - O(N,L) \, \mu_j^{(L)} x' \tag{31b}$$

where

$O(N,L) = 1$ if $N>L$ or $N=L$ and $x \geq x'$,

-1 if $N<L$ or $N=L$ and $x \leq x'$,

and the summation extends to all indices J satisfying

$\min(N,L) \leq J < \max(N,L)$.

The functions (31) give the effective thickness of the material between a plane source placed at depth x in the N-th layer and a parallel plane at depth x' in the L-th layer for the corresponding secondary radiation. The numbers of secondary gamma and X rays absorbed per unit time at depths between x' and x'+dx'

in the L-th layer correlated with nuclear de-excitations in the N-th layer are given by

- Secondary gamma rays resonantly absorbed:

$$RSG^{(N,L)}(y,x')\,dx' = \sec\theta\ \mu_R^{(N)}(y)\ w_0\ \mu_{RS}^{(N,L)} \cdot \left[\int_0^{X^{(N)}} I'\{A_0^{(N,L)}(x,x')\}\ RI^{(N)}(y,x)\,dx\right] dx' \qquad (32a)$$

where $I'(z) \equiv dI(z)/dz$ is the derivative of the function (30).

- Secondary gamma rays absorbed by conventional interactions:

$$CSG^{(N,L)}(y,x')\,dx' = \sec\theta\ \mu_R^{(N)}(y)\ w_0\ \mu_0^{(L)} \cdot \left[\int_0^{X^{(N)}} I'\{A_0^{(N,L)}(x,x')\}\ RI^{(N)}(y,x)\,dx\right] dx'. \qquad (32b)$$

- Secondary X rays of energy E_j:

$$SX^{(N,L)}(y,x')\,dx' = \sec\theta\ \mu_R^{(N)}(y)\ w_j\ \mu_j^{(L)} \cdot \left[\int_0^{X^{(N)}} I'\{A_j^{(N,L)}(x,x')\}\ RI^{(N)}(y,x)\,dx\right] dx'. \qquad (32c)$$

3.2. ELECTRON TRANSPORT.

In the de-excitation of the absorber nuclei after the resonant absorption of a gamma ray, internal conversion (IC) electrons with discrete energies e_1, e_2, ... are emitted. Let u_1, u_2, ... be the corresponding emission probabilities. After the emission of the IC electron of energy e_i, the energy excess of the atom is given away by emission of Auger electrons and/or X rays. As indicated above, we shall neglect the contributions of the low energy Auger electrons resulting from vacancies in the outer shells of the Mössbauer atom. With this approximation, only an Auger electron is emitted in each nuclear de-excitation of the Mössbauer isotopes $^{57}Fe^*$ and $^{119}Sn^*$ (see table I). Furthermore, as the Auger emission can occur only after the IC process, each Auger electron is correlated with an IC electron. Let e'_i and u'_i be the characteristic

energy and emission probability of the Auger electron correlated with the IC electron of energy e_i. For IC electrons coming from outer shells, the subsidiary Auger electron have very small energies and can be ignored. However, it will be simpler to consider them in deriving the theoretical formulae and make $u_i'=0$ in the final expressions.

In order to reduce the number of parameters characterizing the sample we shall introduce some simplifications. As usual, we shall assume that all the electrons are emitted isotropically from the absorber atoms. Although this assumption is not strictly true for photoelectrons (due to the dependence of the photoelectric cross section on the emission angle), its effect on the computed area percentages is expected to be small owing to the relatively low energies used in the Mössbauer experiments [22]. Since photoelectrons contribute to the signal as secondary electrons (less than 10% of the resonant electrons for non-enriched samples) or to the background, this approximation will affect only the less significant contributions to the signal and the background correction (which is negligible for non-enriched samples). Furthermore, as the secondary X and gamma radiations are emitted isotropically, the emission of secondary photoelectrons is nearly isotropical.

All the relevant electron transport properties are included in the weight function T(e,x), which is defined as the probability for an electron generated (isotropically) at a given depth x inside the absorber, with initial energy e, to reach the surface and subsequently be detected. The most recent calculation of weight functions for homogeneous samples has been done by Salvat et al. [16] using the Monte Carlo code MCSDA. The numerical results show that, for any material, the weight function becomes independent of the initial electron energy when depths are measured in units of the Bethe range. Furthermore, if we take metallic iron as the reference material, the weight function for a given material M can be obtained approximately from the energy independent weight function for iron, $T_{Fe}\{x/R(e)\}$, as (see refs. [8] and [16])

$$T_M(e,x) = [T_M(0)/T_{Fe}(0)]\ T_{Fe}\{x/R(e)\} \qquad (33)$$

where R(e) is the Bethe range <u>in iron</u> for electrons of energy e

(see table I). In this way, the weight function for any material is characterized by the single parameter $T_M(0)$ which has to be computed from suitable Monte Carlo methods. The calculations of Salvat et al. [16] show that, for a wide range of materials, $T_M(0) \approx 0.35\ A_M/Z_M$ where A_M is the atomic (or molecular) weight and Z_M the atomic number (or number of electrons in a molecule) of the material M. Eq. (33) states that the electron attenuation on a layer of mass thickness x of the material M is completely equivalent to the attenuation in a layer of iron of the same mass thickness. This fact was previously asserted by Liljequist et al. [14] on the basis of simpler Monte Carlo calculations. However, the results of Salvat et al. [16] show that T(e,x) also depends on the chemical composition of the diffusing material through the factor $T_M(0)$. Weight functions for multilayer absorbers can then be easily obtained from the iron weight function. In order to obtain analytical expressions of the spectral functions, we shall also approximate $T_{Fe}[x/R(e)]$ by a sum of decreasing exponentials

$$\begin{aligned} T_{Fe}(r) = {} & 0.203851\ e^{-31.4112\ r} + 147.585\ e^{-5.34677\ r} - \\ & - 42.1327\ e^{-6.02607\ r} - 106.307\ e^{-5.08245\ r} + \\ & + 1.41436\ e^{-3.12760\ r}. \end{aligned} \tag{34}$$

The parameters in (34) have been obtained from a least squares fitting of the MCSDA results given in ref. [16]. The differences between the data and this fit being lower than the statistical uncertainty of the Monte Carlo results.

One of the most difficult points in the theory is to describe accurately the energy spectrum of the electrons emitted after the photoelectric absorption of an X or gamma ray. As mentioned above, these contribute to the signal as secondary electrons and are responsible for the background defect under the scattering peaks. The emitted photoelectron comes mainly from the innermost atomic shell and, therefore, subsidiary Auger electrons are also emitted and must be taken into account. In some previous theoretical approaches, it has been assumed that, after the photoelectric absorption of a photon of energy E, only a single electron is emitted with initial energy equal to E. As pointed out by Liljequist [8], subsidiary Auger electrons can be ignored because their contribu-

tion will be shadowed by the pairing effect. However, the initial energy of the photoelectrons is lower than the photon energy, the difference being equal to the binding energy of the atomic shell where photoeffect takes place. A somewhat less crude description of photoelectron contributions can be worked out by considering the average range of the emitted photoelectrons as the characteristic parameter in the photoeffect. This average range is written as $\alpha(E)R(E)$ where E is the energy of the absorbed photon and $\alpha(E)<1$ due to the effect of the binding energy of the emitted electrons. The quantity α depends on the photon energy and on the target atom; it should be determined as a properly weighted average of the ranges of all the emitted electrons. For single element materials, $\alpha(E)\approx R(E-U_i)/R(E)$ where U_i is the binding energy of the innermost shell where photoabsorption is energetically possible. In this way, the photoelectron weight function for homogeneous materials reads

$$T_M(E,x) = [T_M(0)/T_{Fe}(0)]\ T_{Fe}\{x/[\alpha(E)R(E)]\}. \qquad (35)$$

As regards to quantitative analysis in ICEMS, inaccuracies in the description of the generation and transport of photoelectrons do not influence appreciably the final results for non-enriched samples. However, this is not true for enriched samples for which errors of a few percent due to these inaccuracies can be expected.

For a multilayer sample, the escaping probability of an electron emitted at a depth x in the N-th layer with initial energy e -that is, the weight function- is given by

$$T^{(N)}(e,x) = [T^{(N)}(0)/T_{Fe}(0)]\ T_{Fe}\{X_T/R(e)\} \qquad (36)$$

with

$$X_T = \sum_{L=1}^{N-1} X^{(L)} + x. \qquad (37)$$

As pointed out in [16], this method introduces some ambiguity in the calculation of ICEMS spectra because we neglect the dependence of the weight function on the composition of the deeper layers in the absorber. Apart from this fact, the validity of eq. (36) is only limited by the accuracy of the scaling properties of

the weight functions which seem to be well established through Monte Carlo calculations [8,16], at least for materials of intermediate atomic number. Inaccuracies of the weight function (36) will produce errors of a few percent in the percentage areas of the simulated ICEMS spectrum. This error is usually smaller than the experimental uncertainty and does not invalidate the quantitative analysis for general purposes.

3.3. ELECTRON COUNTING RATE.

We can now compute the detector counting rate due to gamma rays absorbed in the N-th layer, i.e. the spectral function $S^{(N)}(y)$. We shall consider each contribution separately.

-Primary electrons (PCE and PAE):

For a correlated pair of IC and Auger electrons of energies e_i and e'_i and emission probabilities u_i and u'_i, the probability of obtaining a single count after the resonant absorption of a gamma ray at a depth x inside the N-th layer is given by

$$u_i \, T^{(N)}(e_i,x) + u'_i \, T^{(N)}(e'_i,x) \, [1 - T^{(N)}(e_i,x)] \qquad (38)$$

where the subtracted term gives the decrease of the detector count rate due to the pairing effect.

Clearly, the count rate due to primary electrons emitted in the N-th layer is

$$PE^{(N)}(y) = \sec\theta \; \mu_R^{(N)}(y) \int_0^{X^{(N)}} u^{(N)}(x) \; RI^{(N)}(y,x) \; dx \qquad (39)$$

with

$$u^{(N)}(x) = \sum_i \left[u_i \, T^{(N)}(e_i,x) + u'_i \, T_i^{(N)}(e'_i,x) \, [1 - T_i^{(N)}(e_i,x)] \right]. \qquad (40)$$

Using the results (32a, b and c), the contributions to the count rate due to secondary electrons correlated with nuclear de-excitations in the N-th layer can be easily computed:

-Secondary conversion electrons (GCE):

$$GCE^{(N)}(y) = \sum_{L=1}^{NL} \int_0^{X^{(L)}} u^{(L)}(x') \; RSG^{(N,L)}(y,x') \; dx'. \qquad (41)$$

-Secondary gamma photoelectrons (GPE):

$$GPE^{(N)}(y) = \sum_{L=1}^{NL} \int_0^{X^{(L)}} T^{(L)}(E_0,x')\ CSG^{(N,L)}(y,x')\ dx'. \qquad (42)$$

-Secondary X photoelectrons (XPE):

$$XPE^{(N)}(y) = \sum_{L=1}^{NL} \sum_{j} \int_0^{X^{(L)}} T^{(L)}(E_j,x')\ SX^{(N,L)}(y,x')\ dx'. \qquad (43)$$

-Resonant background:

The resonant background is due to photoelectrons resulting from the conventional absorption of the primary gamma radiation in the considered layer. The corresponding count rate can be written as

$$RBE^{(N)}(y) = RBE^{(N)}(\infty) - BD^{(N)}(y) \qquad (44)$$

where

$$RBE^{(N)}(y) = \sec\theta\ \mu_0^{(N)} \int_0^{X^{(N)}} T^{(N)}(E_0,x)\ Q^{(N)}(x)\ dx \qquad (45)$$

is the resonant background far from the resonances, and $BD^{(N)}(y)$ is the defect of counts due to resonant absorption in the N-th layer:

$$BD^{(N)}(y) = \sec\theta\ \mu_0^{(N)} \int_0^{X^{(N)}} T^{(N)}(E,x)\ Q^{(N)}(x) \cdot \left[R^{(N-1)}(y) - R^{(N)}(y,x)\right] dx$$

$$+ \sec\theta \left[R^{(N-1)}(y) - R^{(N)}(y)\right] \sum_{L=N+1}^{NL} \mu_0^{(L)} \int_0^{X^{(L)}} T^{(L)}(E_0,x)\ Q^{(N)}(x)\ dx. \qquad (46)$$

The term $BD^{(N)}(y)$ vanishes unless there is resonant absorption in the N-th layer. It arises from the fact that a primary gamma ray which is resonantly absorbed cannot suffer photoelectric absorption deeper in the sample. This term reduces the resonant background under the resonance peaks of the N-th layer; the effect is equivalent to an effective reduction of the N-th layer electron count rate.

The spectral function $S^{(N)}(y)$ can now be given as

$$S^{(N)}(y) = PE^{(N)}(y) + GCE^{(N)}(y) + GPE^{(N)}(y) + XPE^{(N)}(y) + RBE^{(N)}(\infty) - BD^{(N)}(y). \quad (47)$$

For reduced energies far from the resonances, the background defect (46) is negligible. Therefore, see eq. (6),

$$SPC^{(N)} = PE^{(N)} + GCE^{(N)} + GPE^{(N)} + XPE^{(N)} - BD^{(N)} \quad (48)$$

Due to the presence of the exponential integral function E_1 in the secondary photon attenuation law (30), the secondary electron contributions to the spectral functions are found as double integrals involving this function whose computation requires a considerable amount of numerical work. These integrals can be computed analytically with good enough approximation if the function I(x) defined in (30) is approximated by a sum of decreasing exponentials as has been done with the electron weight function -see eq. (34)-:

$$I(t) = 0.2634\ e^{-1.122t} + 0.4092\ e^{-1.872t} + 0.3274\ e^{-6.661t}. \quad (49)$$

The relative difference between (30) and (49) is only of a few per cent and, due to the small relative contribution of secondary electrons to the signal, the error introduced into the computed area percentages is found to be negligible. Using this approximation, the spectral functions $SPC^{(N)}(y)$ -eq. (48)- can be written analytically in terms of exponential functions.

4. DISCUSSION.

The reliability of the theory, and also its capabilities in practical applications, can be checked by comparing numerical and experimental results for absorbers of known structure. Measurements of this kind were performed by several groups: Swanson and Spijkerman [1] and Thomas et al. [17] used stainless steel (SS) samples covered with iron layers of different thicknesses. Graham et al. [18] obtained ICEMS spectra of magnetite layers over metallic iron. Tricker et al. [13] used three layer specimens consisting of a SS substratum with a 90 nm of iron evaporated on it and cover-

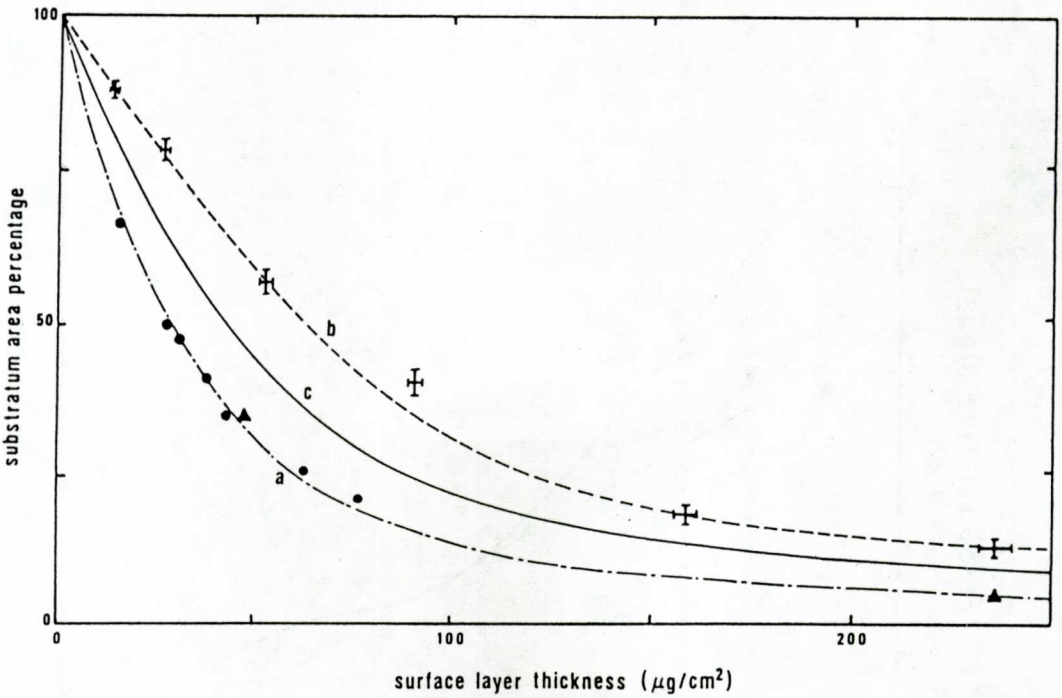

FIGURE 2. Calculated and experimentally measured substratum area percentage for non-enriched absorbers as a function of the surface layer thickness. Curve a refers to the iron-on-stainless steel measurements of Thomas et al. [17] (o) and Swanson and Spijkerman [1] ( ) -see text for details. Curve b corresponds to magnetite-on-iron; the experimental data are from Graham et al. [18]. Curve c gives the area percentage contributed by resonant absorptions deeper than the given thickness for an homogeneous iron absorber, i.e. the U_r function of refs. [6] and [8].

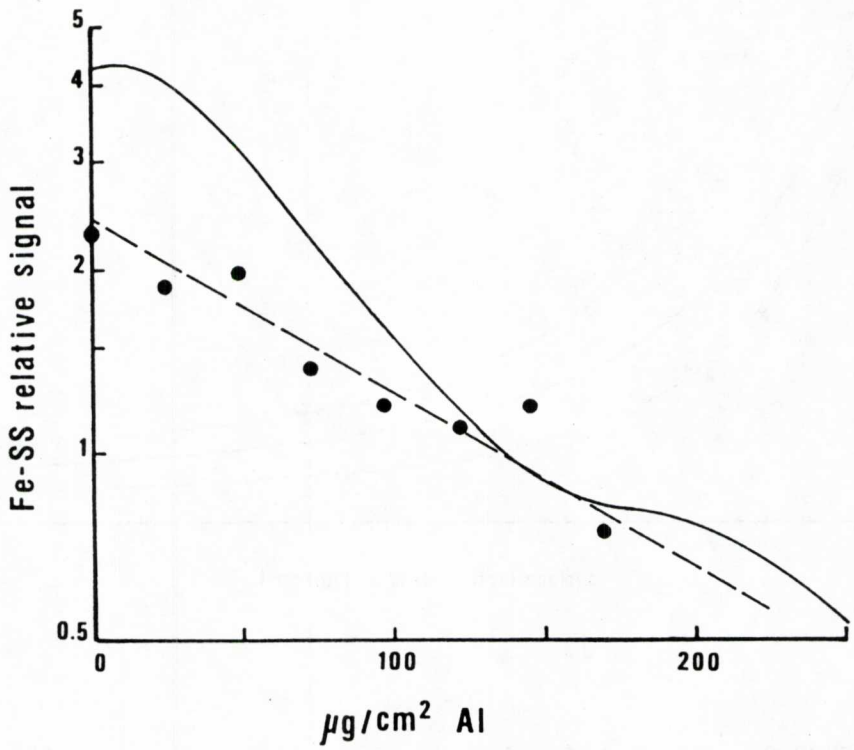

FIGURE 3. Fe-SS relative signal of an SS substratum covered with 90 nm of iron with an overlayer of aluminum as a function of the Al thickness. Experimental data are from Tricker et al. [13]. The continuous curve is the theoretical prediction. The linear fit of Tricker et al. is also shown.

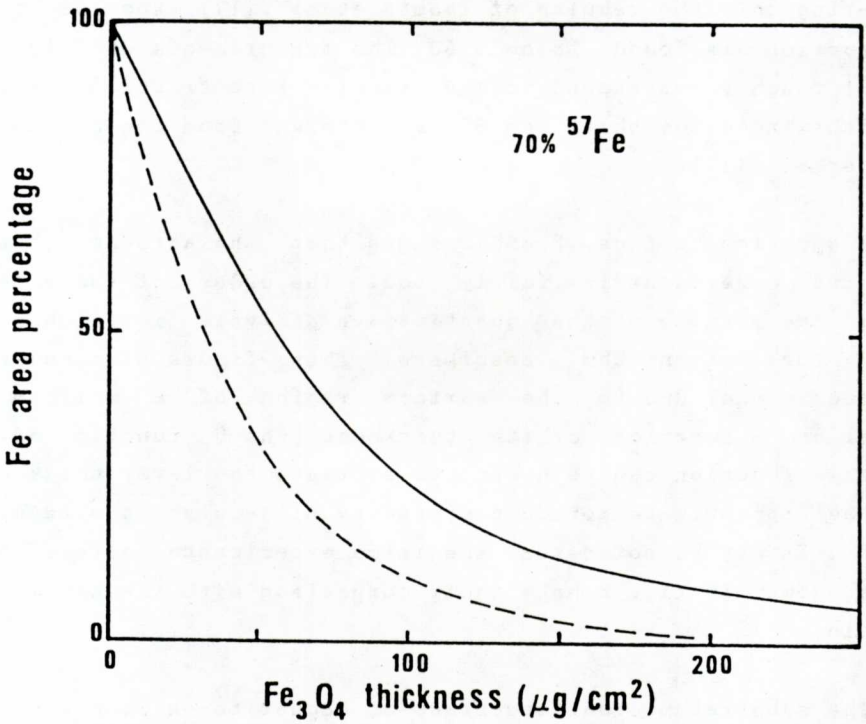

FIGURE 4. Iron area percentage of 70% enriched magnetite-on-iron duplex absorbers as a function of the magnetite layer thickness. ———, present method. -----, Huffman's theory [11,5].

ed with aluminium films of various thicknesses. These experimental results are compared with theoretical estimates in figs. 2 and 3. The SS composition has been assumed to be the same as in ref. [6], namely 71% Fe, 19% Cr and 10% Ni in all the calculations. The recoil-free fraction for metallic iron has been taken to be 0.7. Magnetite and SS recoil- free fractions have been determined by global fitting of the theoretical results to the experimental ones. For magnetite on iron we obtain the value 0.50 of the magnetite recoil free fraction. The ratio of the magnetite and iron recoil-free fractions is 0.7, in agreement with the experimentally measured value used by Liljequist [3] in his most recent calculation. Considering only the results of Thomas et al. [17], the SS recoil-free fraction is found to be 0.63. The measurements of Tricker et al. [13] roughly correspond to a SS recoil free fraction of about 0.5 which indicates that the SS is different from the one used by Thomas et al. [17].

Inspection of figs. 2 and 3 shows that the agreement between theory and experiment is fairly good. The order of the expected error in the results of the quantitative analysis is evidenced in fig. 2 for non-enriched absorbers. This figure also shows the percentage signal due to the surface region of a uniform iron absorber as a function of its thickness (the U_r function of ref. [6]); this function can be useful to estimate the layer thicknesses using the approximate method proposed by Liljequist -see refs. [6] and [8]-. It may be noted that the large experimental errors in the results shown in fig. 3 make their comparison with the theory more uncertain.

The substratum area percentage of magnetite-on-iron absorbers as a function of the magnetite layer thickness computed from the present approach and from Huffman's theory [5,11] are compared in fig. 4. Both results correspond to a 70% ^{57}Fe abundance. Notice the large differences reflecting the gross approximations made by Huffman (cf. fig. 2). Therefore, one must be cautious with the use of the approximate theories [9-11], which can only be useful to provide a first approximation to the quantitative analysis.

The above results show that the present state of the theory makes the quantitative analysis workable in ICEMS. The magnitude of the errors introduced by the theory seems to be in the order of a few percent. However, it should be stressed that the global error in the result of a quantitative analysis using the present theory can be much larger due to uncertainties in the experimental area percentages.

The theory described above can be used for practical quantitative analysis of multilayer samples. It is assumed that the composition and order in depth of the different phases in the absorber are known, i.e. a good qualitative description of the sample is required before attempting quantitative analysis. The layer compositions can be found by inspection of measured spectrum. As quite a number of solid phases have well known characteristic Mössbauer spectra, the partial signals in the measured spectrum can serve as finger-prints indicating the presence of the corresponding phases. Although the order is evident when the history of the sample is known in detail, e.g. in oxidation problems, it may be doubtful in many situations (e.g. when analysing weathered minerals or grossly corroded metals or alloys). In this last case, the empirical methods developed by the group of Tricker [23,24] to distinguish between substratum and overlayer signals can be of great value to determine the correct order in depth of the present phases. Once the qualitative structure of the sample is known, quantitative analysis, i.e. determination of the thicknesses of the distinct layers, can be performed through numerical fitting of the computed area percentages to the observed ones.

APPENDIX A. Radiations emitted in the nuclear de-excitation.

Since the Mössbauer nuclei are surrounded by the atomic electrons, the excited nucleus can de-excite by emission of an Internal Conversion (IC) electron as well as by gamma emission. In the IC process with the i-th atomic shell, the energy of the nuclear transition, E_0, is transferred to an electron in this shell which leaves the atom with a kinetic energy $e_i=E_0-B_i$ where B_i is the binding energy of the i-th shell. The partial IC coefficient

for the i-th shell, α_i, is defined as $\alpha_i=N_i/N_0$ where N_i and N_0 are the numbers of IC electrons (coming from the i-th atomic shell) and gamma rays emitted in a sample containing a large number of excited nuclei. The total IC coefficient α is defined as the sum of the partial IC coefficients for each atomic subshell: $\alpha=\alpha_K+\alpha_L+\alpha_M+\ldots$ It should be noted that IC is most likely to occur in the innermost shell (K shell in ^{57}Fe, L shell in ^{119}Sn), the partial IC coefficients of the outer atomic shells being usually small in comparison with the inner shells.

After the IC process, the residual ion is left in an excited state with a vacancy in the i-th shell (usually an inner shell). In the de-excitation of the ion, the vacancy is filled by a transition of an electron from an outer shell, say the j-th one (ij transition). The energy excess, $E_X=B_i-B_j$, is either emitted as a characteristic X ray or transferred to an electron in the k-th shell which leaves the ion with kinetic energy $E_e=E_X-B_k$. This last process is known as Auger effect and the ejected electron is referred to as an ij-k Auger electron. The probability of X ray emission in the ij transition is given by the fluorescence yield $(FY)_{ij}$. Clearly, the probability of Auger emission after an ij transition is $1-(FY)_{ij}$. From the knowledge of B_i, α_i and $(FY)_{ij}$ it is possible to determine the kind of radiations emitted in the de-excitation of a Mössbauer nuclei as well as their energies and emission probabilities. For example, a vacancy in the K shell of the Fe atom can be filled by an electron of the L shell; the energy B_K-B_L is given off by emission of either a K_α X ray (with probability $(FY)_{KL}$) or a KL-j Auger electron (with probability $1-(FY)_{KL}$). The vacancy produced by the Auger process is then filled by electrons from higher shells and additional characteristic X rays and Auger electrons are emitted. The process continues (Auger cascade) until the initial energy B_K-B_L is released. From a given inner vacancy a large number of different Auger transitions may result. In addition to the difficulties due to the complexity of the de-excitation process, the fluorescence yields of the possible transitions of the residual ion are not usually known except for vacancies in the K shell [25] and we need to resort to an approximate description. Additional problems result from the fact that the L shell fluorescence yield depends on the mode of vacancy production [25].

^{57}Fe: The experimental electron binding energies for the neutral Fe atom given by Bearden and Burr [26] will be used. We shall adopt the theoretical IC coefficients for the 14.4 transition of the ^{57}Fe Mössbauer isotope computed by Raff et al. [27]. These partial ICC are: α_K=7.675, α_L=0.784, α_M=0.115. The resulting total IC coefficient is α=8.574 which agrees well with the experimental value 8.26±0.19. The K shell fluorescence yield is taken to be $(FY)_K$=0.34 [28] which agrees with a semiempirical formula [25] giving $(FY)_K$ as a function of the atomic number with an accuracy of about 0.05. Auger transitions other than KL-L are two orders of magnitude less probable than these ones. Then we shall assume that all the vacancies in the K shell are filled with L electrons. X rays and Auger electrons resulting from a vacancy in the L shell have energies lower than 1 keV. Those low energy Auger electrons (and the secondary photoelectrons produced by the soft X rays) are strongly attenuated inside the absorber and may be ignored in the calculation of ICEMS spectra. The characteristics of the main radiations emitted in the de-excitation of the ^{57}Fe nuclei derived from the preceding data are given in table I.

^{119}Sn: The electron binding energies have also been taken from the experimental averages of Bearden and Burr [26]. The theoretical total IC coefficient for the 23.8 keV transition [27] is α=5.08 in good agreement with the experimental value 5.13±0.15. As the partial IC coefficient for the shells that are more external than the L one contribute only a small percentage to α, we shall take $\alpha_L=\alpha$ and ignore IC processes in outer shells. As indicated above, fluorescence yields for the L shell are uncertain. By the lack of more rigorous data we shall take $(FY)_L$=0.12 (see fig. 6 in ref. [25]) and consider only LM-M Auger electrons and X rays produced in LM transitions. As in the case of iron, the electrons resulting from other transitions have energies that are lower than 1 keV and do not contribute appreciably to the ICEMS spectrum. The energies and emission probabilities of the main radiations ejected from the Mössbauer atom derived from these data are shown in table I.

REFERENCES.

1. K. R. Swanson and J. J. Spijkerman, J. Appl. Phys. 41 (1970) 3155.
2. M. J. Tricker, in **Mössbauer Spectroscopy and its Chemical Applications**, Advances in Chemistry Series 194, J. G. Stevens and G. K. Shenoy Eds. (American Chemical Society, Washington DC, USA, 1981) p63.
3. D. Liljequist, Scanning Electron Microscopy (1983) III 997.
4. G. W. Simmons, E. Kellermen and H. Leidheiser Jr., Corrosion 29 (1973) 227
5. G. P. Huffman and H. H. Podgurski, Oxidation of metals 10 (1976) 377.
6. F. Salvat and J. Parellada, Nucl. Instr. and Meth. B1 (1984) 70.
7. F. A. Deeney and P. J. McCarthy, Nucl. Instr. and Meth. 166 (1979) 491.
8. D. Liljequist, USIP Report 80-07 (1980).
9. R. A. Krakowski and R. B. Miller, Nucl. Instr. and Meth. 100 (1972) 73.
10. J. Bainbridge, Nucl. Instr. and Meth. 128 (1975) 531.
11. G. P. Huffman, Nucl. Instr. and Meth. 138 (1976) 267.
12. V. E. Cosslett and R. N. Thomas, Brit. J. Appl. Phys. 15 (1964) 883.
13. M. J. Tricker, L. A. Ash and T. E. Cranshaw, Nucl. Instr. and Meth. 143 (1977) 307.
14. D. Liljequist, C. Bohm and T. Eckdahl, Nucl. Instr. and Meth. 177 (1980) 495.
15. D. Liljequist, Nucl. Instr. and Meth. 179 (1981) 617.
16. F. Salvat, R. Mayol, J. D. Martinez and J. Parellada, Nucl. Instr. and Meth. B6 (1985) 547.
17. J. M. Thomas, M. J. Tricker and A. Winterbottom, J. Chem. Soc., Faraday II, 71 (1975) 1708.
18. M. J. Graham, D. F. Michell and D. A. Channing, Ox of Metals 12 (1978) 247.
19. J. H. Hubbell, Int. J. Appl. Radiat. Isot. 33 (1982) 1279.

20. International Tables for X-ray Crystallography vols. 3 and 4, J. A. Ibers and W. C. Hamilton Eds. (The Kinoch Press, Birmingham, England, 1974).
21. Handbook of Mathematical Functions, M. Abramowitz and I. A. Stegun Eds. (Dover, New York, 1972).
22. C. M. Davisson and R. D. Evans, Rev. Mod. Phys. 24 (1952) 79.
23. M. J. Tricker, A. G. Freeman, A. P. Winterbottom and J. M. Thomas, Nucl. Instr. and Meth. 135 (1976) 117.
24. M. J. Tricker, L. Ash and W. Jones, Surface Sci. 79 (1979) L333.
25. I. Bergström and C. Nordling, Alpha-, Beta- and Gamma-ray Spectroscopy, Ed. by K. Siegbahn (North-Holland, Amsterdam, 1968) vol.2 p.1523.
26. J. A. Bearden and A. F. Burr, Rev. Mod. Phys. 39 (1967) 125.
27. U. Raff, K. Alder and G. Baur, Helvetica Physica Acta 45 (1972) 427.
28. W. Rubinson and K. P. Gopinathan, Phys. Rev 170 (1968) 969.